Antiferromagnetic $S = 1/2$ Spin Chain Driven by p-Orbital Ordering in CsO_2

Syarif Riyadi,[1] Baomin Zhang,[2] Robert A. de Groot,[1,2] Antonio Caretta,[1] Paul H. M. van Loosdrecht,[1] Thomas T. M. Palstra,[1] and Graeme R. Blake[1,*]

[1]*Zernike Institute for Advanced Materials, University of Groningen, Nijenborgh 4, 9747 AG Groningen, The Netherlands*
[2]*Radboud University, Institute for Molecules and Materials, Heyendaalseweg 135, 6525 AJ Nijmegen, The Netherlands*

(Received 13 February 2012; published 25 May 2012)

We demonstrate, using a combination of experiment and density functional theory, that orbital ordering drives the formation of a one-dimensional (1D) $S = 1/2$ antiferromagnetic spin chain in the 3D rocksalt structure of cesium superoxide (CsO_2). The magnetic superoxide anion (O_2^-) exhibits degeneracy of its $2p$-derived molecular orbitals, which is lifted by a structural distortion on cooling. A spin chain is then formed by zigzag ordering of the half-filled superoxide orbitals, promoting a superexchange pathway mediated by the p_z orbitals of Cs^+ along only one crystal direction. This scenario is analogous to the $3d$-orbital-driven spin chain found in the perovskite $KCuF_3$ and is the first example of an inorganic quantum spin system with unpaired p electrons.

DOI: 10.1103/PhysRevLett.108.217206 PACS numbers: 75.25.Dk, 71.20.−b, 75.10.Pq, 78.30.−j

Research into magnetic materials has begun to extend beyond d and f-block electron systems to those in which magnetism arises from unpaired spins in p orbitals [1]. Such compounds are relatively scarce because the more extended p orbitals result in a tendency toward electron pairing in covalent bonds. Perhaps the most suitable model systems for the study of p-electron magnetism are the alkali metal superoxides (AO_2), which form ionic crystals adopting structures related to rocksalt [2]. The valence electrons in AO_2 reside in states that are almost purely of oxygen character. In the superoxide anion (O_2^-), three electrons occupy a pair of degenerate antibonding π^* molecular orbitals; thus, there is one unpaired spin ($S = 1/2$). Accordingly, these compounds are susceptible to structural distortions that split the π^* energy levels and lift the orbital degeneracy [3], similar to the Jahn-Teller effect for degenerate d orbitals. Orbital ordering (OO) similar to that found in transition-metal systems [4] may then be expected. The linear O_2^- anion has an additional orientational degree of freedom compared to JT-active transition-metal species and the orbital degeneracy in AO_2 compounds is lifted by cooperative tilting and displacement of the anions [2,5].

It is becoming increasingly clear that AO_2, as well as the A_2O_3 sesquioxides [6,7] and the O_2MF_6 (M = Sb, Pt) dioxygenyl compounds [8], can be considered within the framework of correlated electron systems. In AO_2, direct antiferromagnetic (AFM) exchange can occur when the axes of nearest-neighbor O_2^- anions are parallel and the lobes of their half-occupied π^* orbitals point toward each other [9]. It is also probable that superexchange via either the empty s orbitals or filled p orbitals of the A^+ cations can occur, which probably determines the ground-state magnetic structures of KO_2, RbO_2, and CsO_2, reported to be AFM below 7.1 K, 14.7 K, and 9.6 K, respectively [10,11]. Only the magnetic structure of KO_2 has been studied by neutron diffraction. Here, spins in the pseudotetragonal ab plane are aligned in ferromagnetic (FM) fashion, while planes are AFM coupled along the c axis [12]. Electron paramagnetic resonance (EPR) studies have suggested that the same magnetic structure is present in RbO_2 and CsO_2, and that the magnetic easy axis is orthogonal to the anion axis in all AO_2 [11]. These experimental observations, made more than three decades ago, have recently inspired further theoretical work on KO_2 and RbO_2 [13–15] focused on the possible ground-state OO configurations and their influence on spin ordering. Although no consistent picture has yet emerged, it is becoming clear that the coupling in AO_2 between spin, orbital, and lattice degrees of freedom (the latter including the tilting of the anions) is as relevant as for strongly correlated transition-metal systems. Here, we reinvestigate the magnetic properties of CsO_2 and show that OO drives the formation of a 1D AFM spin chain, the clearest demonstration thus far of correlated electron physics in an inorganic p-electron spin system.

Polycrystalline CsO_2 was prepared by passing dry oxygen gas through a solution of Cs metal in liquid ammonia at −65 °C for 2 h. The solution was then warmed to remove ammonia, leaving yellow CsO_2 powder. Magnetic measurements were performed on samples sealed in vacuum inside glass tubes using a Quantum Design MPMS-XL 7 magnetometer. X-ray powder diffraction (XRPD) was performed using a Huber G670 diffractometer operating with Cu $K\alpha_1$ radiation. The sample was sandwiched between two Mylar films to avoid exposure to air. The XRPD data were analyzed using the General Structure Analysis System (GSAS) software [16]. Raman spectroscopy was performed in a backscattering configuration using a liquid nitrogen-cooled charge coupled device (CCD) connected to a three-grating micro-Raman spectrometer (T64000 Jobin Yvon). Samples were contained on a copper plate in thermal contact with a cold finger inside a cryocooled,

evacuated chamber. A laser power density of 0.05 mW/μm^2 was used. Density functional theory (DFT) calculations were carried out from first principles using the generalized gradient approximation (GGA) + U method with $U = 4.0$ eV, as implemented in the Vienna *ab initio* simulation package (VASP) [17]. More details are given in the Supplemental Material [18].

The dominant feature in the magnetic susceptibility of polycrystalline CsO_2 is a broad maximum centered at ~28 K [Fig. 1(a)]. A similar feature was previously observed by Zumsteg *et al.* [10], who remarked only that considerable magnetic order remained above $T_N = 9.6$ K.

Such a maximum is a typical indication of low-dimensional magnetic ordering [19]. The spins in AO_2 can rotate in the plane perpendicular to the molecular axis, but EPR shows only moderate anisotropy of the g tensor [11,20]; thus, we can treat CsO_2 as an isotropic (Heisenberg) spin system. The susceptibility maximum was fitted using the $S = 1/2$ square-lattice Heisenberg model formulated by Keith *et al.* [21]. There are three variable parameters in this model: the exchange constant for a particular crystal direction J/k_B, the ratio α between two orthogonal exchange constants on a square lattice ($J' = \alpha J$), and the Curie constant. For 2D AFM ordering, $J = J'$ and $\alpha = 1$; for an AFM spin chain, $\alpha = 0$. This model can also be applied to 2D systems incorporating mixed AFM and FM interactions, for which $-1 \leq \alpha < 0$. The best fit to our data is shown in Fig. 1(a), which yielded $J/k_B = 20.27$ K, $\alpha = 0$, and $C = 0.325$. The zero value of α implies that CsO_2 is essentially an AFM spin chain. Fits performed with fixed nonzero positive or negative values of α were visibly worse. We also fitted the susceptibility maximum using an alternative expression reported by Feyerherm *et al.* [22], based on the original formulation for a $S = 1/2$ Heisenberg AFM chain by Bonner and Fisher [19]. We obtained $J/k_B = 20.0$ K, in good agreement with the model of Keith *et al.* [21]. Both models fitted the data equally well between 15 K and 70 K, at which a small anomaly associated with a structural transition (see below) is apparent. The spin chain appears to persist in applied fields up to at least 40 kOe [18]. A Curie-Weiss fit to the inverse susceptibility above 150 K [Fig. 1(b)] yielded an effective moment of 2.03 μ_B. This is significantly higher than the expected spin-only value for $S = 1/2$ and is consistent with previous reports on CsO_2 and other AO_2 [10,20], suggesting unquenched orbital momentum. The fitted Weiss constant of $\theta = -40.3$ K, which corresponds to $\sim 4T_N$, is more evidence for the quantum AFM nature of CsO_2.

Long-range 3D AFM ordering in CsO_2 was previously reported below $T_N = 9.6$ K on the basis of specific heat, magnetic susceptibility, and EPR measurements [11,10]. We observe a magnetic susceptibility anomaly at ~9.5 K [Fig. 1(b)] and the spin chain models no longer fit the data below ~15 K, supporting a transition to 3D ordering. The low-temperature susceptibility tail below 7 K is likely due to residual spins; a fit to the Curie law yielded a concentration of ~8% $S = 1/2$ disordered spins.

At room temperature, the XRPD pattern of CsO_2 is consistent with the previously reported tetragonal average structure (space group $I4/mmm$) [23]. However, Raman spectroscopy (see below) demonstrates that the true symmetry is lower. An impurity phase ($CsOH.H_2O$, ~20% by weight) was also present but does not contribute to the magnetic response. Splitting of the CsO_2 XRPD peaks with $h \neq k$ was observed below 70 K (see Fig. 2), consistent with a transition to orthorhombic symmetry. However, Rietveld refinements were rather insensitive to the oxygen positions and we were unable to determine details of the low-temperature structure. An earlier XRD study on CsO_2 single crystals reported a tetragonal-to-orthorhombic transition at the higher temperature of 190 K [23], below which incommensurate satellite reflections also appeared. No such peaks were apparent in our data. It was previously reported that different solution-grown CsO_2 single crystals from the same batch did not always exhibit a

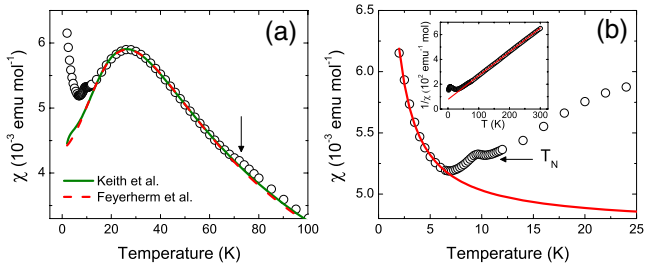

FIG. 1 (color online). (a) Magnetic susceptibility versus temperature for polycrystalline CsO_2, measured on warming in a field of 10 kOe after cooling in the same field. Fits to the models of Keith *et al.* [21] (green solid line) and Feyerherm *et al.* [22] (red dashed line) are shown. The arrow indicates an anomaly at 70 K. (b) Low-temperature magnetic susceptibility showing T_N and a fit of the low-temperature susceptibility tail to the Curie law. A Curie-Weiss fit to the inverse susceptibility above 150 K is shown in the inset.

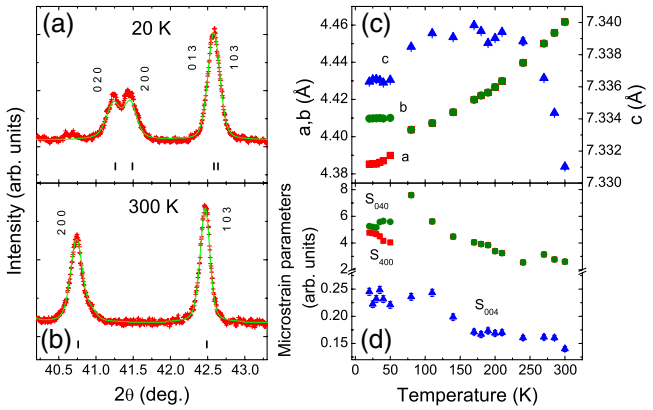

FIG. 2 (color online). (a),(b) 200 and 103 XRPD peaks in the tetragonal and orthorhombic regimes. (c) Evolution of lattice parameters and (d) selected microstrain peak-broadening parameters with temperature.

tetragonal-orthorhombic transition [24], which suggests a sensitive dependence of the structure on oxygen stoichiometry. The evolution of the lattice parameters with temperature of our sample is shown in Fig. 2(c). Apart from the phase transition at ~70 K, the other noteworthy feature is a decrease of the c parameter above 200 K. This might be due to increasing librational freedom of the anions in the a and b directions on heating. The c axis also shortens on cooling below ~100 K, suggestive of coherent anion tilting away from the axis. The refinement of anisotropic microstrain peak-broadening parameters, using the Stephens formulation [25], was necessary at all temperatures to fit the peak profiles. The S_{400} and S_{040} parameters were much larger than S_{004} [Fig. 2(d)], indicating either a degree of disorder or smaller coherently diffracting domain size in the pseudotetragonal basal plane.

Raman spectroscopy provided greater insight into the crystal structure. For the tetragonal average structure, three Raman active modes are apparent [Fig. 3(a)]. The stretching mode of O_2^- is observed at 1134 cm^{-1}, which agrees well with the previously reported 1137 cm^{-1} [26]. The broad peaks at 75 cm^{-1} and 205 cm^{-1} are probably a phonon mode involving the Cs cations and a O_2^- librational mode, respectively (see below). The presence of the 75 cm^{-1} mode is incompatible with $I4/mmm$ symmetry [18] and is evidence that the local symmetry is lower, as previously inferred from single-crystal XRD measurements [23].

Figure 3(b) shows the Raman spectrum at 4.5 K. Four peaks are apparent at low wave numbers, the origin

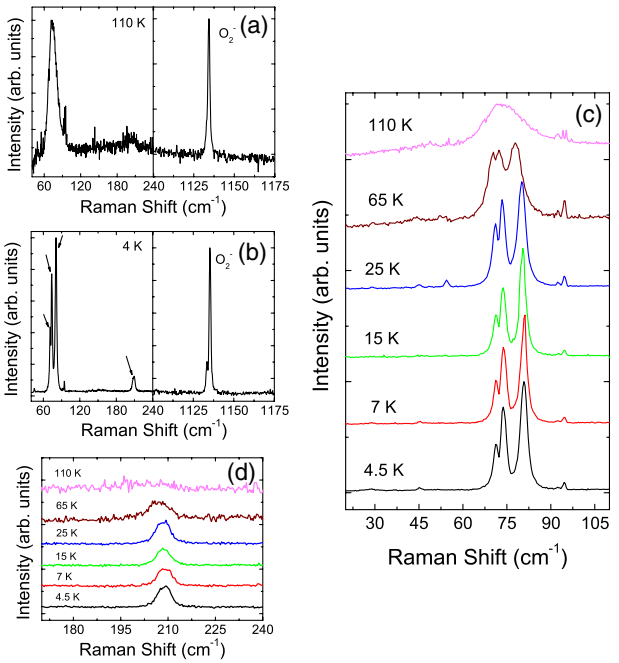

FIG. 3 (color online). Raman spectra of CsO_2 at (a) 110 K and (b) 4.5 K. (c) Raman modes associated with the interlayer motion of Cs and (d) librational mode of O_2^- as a function of temperature.

of which was investigated by optimizing the orthorhombic structure of CsO_2 using DFT calculations without symmetry constraints. By using a supercell doubled along all three axes and the lattice parameters determined by XRPD at 20 K, we obtained two degenerate solutions. In the first structural solution, the anions are tilted by ~5° from c toward the basal plane diagonal, as shown in Fig. 4(b). The tilt directions are staggered along b and uniform along a, corresponding to a doubled b axis. The tilting of anions in the $z = 1/2$ layer of the supercell (which is the same as that in the $z = 1/4$ layer) is opposite to the tilting of anions in the $z = 0$ layer (the same as that in the $z = 3/4$ layer). Thus, a staggered pattern is formed when viewed along c and the c axis is also doubled. Within the ab plane there are staggered shifts of the Cs cations in the a direction, such that along b the cations form a zigzag arrangement. This is likely a consequence of the staggered anion tilts. In the second structural model the $z = 0$ and $z = 1/2$ layers are identical to those in the first structure, but the patterns of Cs shifts and anion tilts in these two layers are rotated by 90° in the $z = 1/4$ and $z = 3/4$ layers, respectively, such that the tilts become staggered along a rather than along b and the a axis is also doubled. This unit cell would be metrically tetragonal because overall there is no structural anisotropy in the ab plane. However, we observe a metrically orthorhombic cell (Fig. 2); thus, we favor the first model. Calculations of the Raman modes were carried out in VASP using the $a \times 2b \times 2c$ supercell [18]. Four Raman modes at low wave numbers were obtained: 66 cm^{-1}, 67 cm^{-1}, 75 cm^{-1}, and 200 cm^{-1}, which agree well with the experimental spectrum. The first three modes are associated with interlayer motions of the Cs cations along the c direction [18], and the broad feature observed at 209 cm^{-1} is the librational mode ("swing-like" motion) of O_2^-. Finally, the calculated O_2^- stretching mode at 1120 cm^{-1} agrees well with the observed mode at 1135 cm^{-1}. Figure 3(c) shows the temperature dependence of the three low wave-number Cs modes, which merge to become a single broad peak

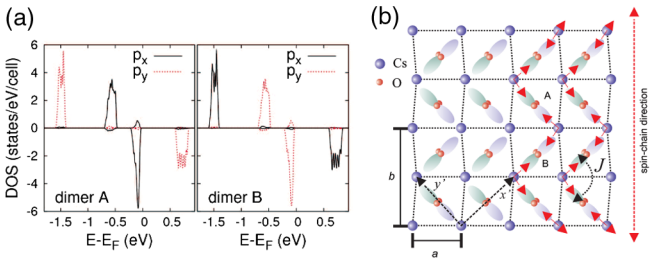

FIG. 4 (color online). (a) Partial oxygen DOS for anions A and B along the b axis in the $z = 0$ layer below 70 K. Because of the AFM configuration, the spin-up and spin-down DOS for anions in the $z = 1/4$ layer is reversed compared to the DOS shown here. (b) ab-plane view of the optimized structure of CsO_2 below 70 K showing anion tilting and ordering of the half-occupied π_x^* and π_y^* orbitals.

above the 70 K structural phase transition. The O_2^- librational mode broadens and weakens between 65 K and 110 K but does not disappear completely [Fig. 3(d)].

The phase transition at ~70 K results in OO, which is apparent from the site-projected partial oxygen DOS shown in Fig. 4(a) for two adjacent anions A and B along the b axis of the optimized structure in Fig. 4(b). The four peaks in the DOS for each anion correspond to the spin-up and spin-down states of the two π^* orbitals, three of which are fully occupied and one of which, above the Fermi level (E_f), is empty. The states in the energy range -1 to 0 eV correspond to a filled π_x^* orbital for dimer A and a filled π_y^* orbital for dimer B. Here, x and y refer to the coordinate system indicated by axes x' and y' in Fig. 4(b), which are at ~45° to the unit cell axes a and b. For any given dimer, the π_y^* orbital is fully occupied on two nearest-neighbor dimers within the pseudotetragonal plane and the π_x^* orbital is fully occupied on the other two. This corresponds to a zigzag configuration of alternating half-filled π_x^* and π_y^* orbitals along the b axis, as shown in Fig. 4(b) (the anion axes tilt by ~5° from the c axis and are almost perpendicular to the plane of the picture.)

The lobes of the magnetic orbitals do not point toward each other; thus, direct exchange will be weak and possible superexchange pathways via Cs must be examined. The occupied Cs p_z orbitals have the correct orientation to mediate coupling along the pathways marked by red arrows in Fig. 4(b), whereas no obvious superexchange pathway is available in the perpendicular direction. The Cs p_z orbitals lie at energies between -8.5 eV and -5 eV with respect to E_f [18]. The sign of the superexchange along b is AFM according to the Kugel-Khomskii picture [27]. The unit cell is doubled in the c direction: when site A at $z = 0$ in Fig. 4(b) has a half-occupied π_y^* orbital, the corresponding site at $z = 1/2$ has a half-occupied π_x^* orbital. Linear superexchange pathways along c of the type $O_2\pi_x^*$-Csp_x-$O_2\pi_x^*$ are thus prevented. The result is an AFM spin chain in the b direction.

The anion tilting and OO configuration in Fig. 4(b) is analogous to that calculated for KO_2 by Nandy *et al.* [15]. Although the interatomic distances along the b direction in KO_2 are shorter, the magnetic susceptibility does not suggest low-dimensional ordering [10]. It is possible that the superexchange pathway along b is disrupted by the much greater anion tilting in KO_2. Similarly, no spin chain seems to form in RbO_2, despite the crystal structure being very similar to CsO_2 [2]. This may be due to a different ground state OO configuration, calculated to be staggered along both basal plane axes with orbital lobes pointing between the Rb^+ cations [14]. We also note that the relevant p-levels of Rb and K lie significantly deeper than for Cs [28]. The marcasite phase of NaO_2 below 196 K might exhibit a spin chain along the c axis due to strong AFM direct exchange between anions [9]. A coupling constant of $J = -370$ K was calculated for the situation where the lobes of half-occupied orbitals on nearest neighbors point toward each other [29]. The magnetic susceptibility should thus rise with temperature without reaching the typical broad maximum associated with a spin chain; this result has been experimentally observed [10,29], but the data were not fitted to any model and OO has not been confirmed.

Although several examples of AFM p-electron spin chains are known in organic charge-transfer salts, these are a consequence of low structural dimensionality [30]. The closest analogy to CsO_2 is found in the d-electron spin chain $KCuF_3$ [31]. In this tetragonal perovskite, the distances between Cu^{2+} cations are similar along the three principal crystallographic axes (4.14, 4.14, and 3.93 Å). A Jahn-Teller distortion removes the Cu^{2+} orbital degeneracy, breaking the octahedral symmetry and favoring an alternating occupation of half-occupied $d_{x^2-z^2}$ and $d_{y^2-z^2}$ orbitals in the ab plane. The lobes of the half-occupied orbitals on neighboring cations are orthogonal to each other in the ab plane; thus, superexchange between nearest neighbors is extremely weak. In contrast, the lobes of both orbitals overlap with the fluorine p_z orbitals in the c direction, allowing superexchange along a linear pathway. An AFM spin chain is formed with $J_c/J_a = -100$ [32]. At ~40 K, the spin chain gives way to 3D A-type AFM order [33]. An explanation for this has recently been proposed by Lee *et al.* [34], who calculated that the half-occupied orbitals can more accurately be described as hybrids of $d_{x^2-z^2}$ and $d_{y^2-z^2}$, two distinct and almost degenerate states of which exist in the spin-chain regime. One hybrid state favors AFM order in-plane and the other FM order in-plane, and rapid fluctuations between the two states occur. A structural distortion involving short-range-ordered rotations of the octahedra takes place at ~40 K, stabilizing the AFM hybrid state. In CsO_2, the 3D AFM ordering that sets in below 9.6 K requires the availability of superexchange pathways along both a and c. Our Raman data (Fig. 3) reveal no obvious structural change down to 4.5 K; thus, the OO configuration and alternative superexchange pathways should be studied in more detail.

In conclusion, our observation of a $S = 1/2$ AFM spin chain in CsO_2 that is driven by OO is the clearest demonstration yet of correlated electron physics at play in an inorganic, open p-shell system. Our study shows that the concepts of orbital physics developed for transition metals are also valid for main-group systems with orbital degeneracy.

We thank G. A. de Wijs, S. Giriyapura, and P. Mahadevan for useful discussions. This Letter is part of the research program of the Foundation for Fundamental Research on Matter (FOM), which is financially supported by the Netherlands Organisation for Scientific Research (NWO).

*G.R.Blake@rug.nl

[1] O. Volnianska and P. Boguslawski, J. Phys.: Condens. Matter **22**, 073202 (2010).
[2] W. Hesse, M. Jansen, and W. Schnick, Prog. Solid State Chem. **19**, 47 (1989).
[3] I. Solovyev, New J. Phys. **10**, 013035 (2008).
[4] Y. Tokura and N. Nagaosa, Science **288**, 462 (2000).
[5] S. Riyadi, S. Giriyapura, R. A. de Groot, A. Caretta, P. H. M. van Loosdrecht, T. T. M. Palstra, and G. R. Blake, Chem. Mater. **23**, 1578 (2011).
[6] J. Winterlik, G. H. Fecher, C. A. Jenkins, C. Felser, C. Mühle, K. Doll, M. Jansen, L. M. Sandratskii, and J. Kübler, Phys. Rev. Lett. **102**, 016401 (2009).
[7] J. Winterlik, G. H. Fecher, C. A. Jenkins, S. Medvedev, C. Felser, J. Kübler, C. Mühle, K. Doll, M. Jansen, T. Palasyuk, I. Trojan, M. I. Eremets, and F. Emmerling, Phys. Rev. B **79**, 214410 (2009).
[8] M. Kim and B. I. Min, Phys. Rev. B **84**, 073106 (2011).
[9] S. D. Mahanti and G. Kemeny, Phys. Rev. B **20**, 2105 (1979).
[10] A. Zumsteg, M. Ziegler, W. Känzig, and M. Bösch, Z. Phys. B **17**, 267 (1974).
[11] M. Labhart, D. Raoux, W. Känzig, and M. A. Bösch, Phys. Rev. B **20**, 53 (1979).
[12] H. G. Smith, R. M. Nicklow, L. J. Raubenheimer, and M. K. Wilkinson, J. Appl. Phys. **37**, 1047 (1966).
[13] M. Kim, B. H. Kim, H. C. Choi, and B. I. Min, Phys. Rev. B **81**, 100409 (2010).
[14] E. R. Ylvisaker, R. R. P. Singh, and W. E. Pickett, Phys. Rev. B **81**, 180405 (2010).
[15] A. K. Nandy, P. Mahadevan, P. Sen, and D. D. Sarma, Phys. Rev. Lett. **105**, 056403 (2010).
[16] A. C. Larson and R. B. von Dreele, Los Alamos National Laboratory LAUR Report 2004, No. 86-748, 2004.
[17] G. Kresse and J. Hafner, Phys. Rev. B **47**, 558 (1993).
[18] See Supplemental Material at http://link.aps.org/supplemental/10.1103/PhysRevLett.108.217206 for DFT calculations and magnetic properties as a function of applied field.
[19] J. C. Bonner and M. E. Fisher, Phys. Rev. **135**, A640 (1964).
[20] P. D. C. Dietzel, R. H. Kremer, and M. Jansen, J. Am. Chem. Soc. **126**, 4689 (2004).
[21] B. C. Keith, C. P. Landee, T. Valleau, M. M. Turnbull, and N. Harrison, Phys. Rev. B **84**, 104442 (2011).
[22] R. Feyerherm, S. Abens, D. Gunther, T. Ishida, M. Meissner, M. Meschke, T. Nogami, and M. Steiner, J. Phys.: Condens. Matter **12**, 8495 (2000).
[23] M. Ziegler, M. Rosenfeld, W. Känzig, and P. Fischer, Helv. Phys. Acta **49**, 57 (1976).
[24] M. Rosenfeld, M. Ziegler, and W. Känzig, Helv. Phys. Acta **51**, 298 (1978).
[25] P. W. Stephens, J. Appl. Crystallogr. **32**, 281 (1999).
[26] J. B. Bates, G. E. Boyd, and M. H. Brooker, Chem. Phys. Lett. **16**, 391 (1972).
[27] K. I. Kugel and D. I. Khomskii, Sov. Phys. Usp. **25**, 231 (1982).
[28] *Photoemission in Solids I: General Principles*, edited by M. Cardona and L. Ley (Springer-Verlag, Berlin, 1978).
[29] S. D. Mahanti and A. U. Khan, Solid State Commun. **18**, 159 (1976).
[30] M. Dressel, Naturwissenschaften **94**, 527 (2007).
[31] S. Kadota, I. Yamada, S. Yoneyama, and K. Hirakawa, J. Phys. Soc. Jpn. **23**, 751 (1967).
[32] S. K. Satija, J. D. Axe, G. Shirane, H. Yoshizawa, and K. Hirakawa, Phys. Rev. B **21**, 2001 (1980).
[33] M. T. Hutchings, E. J. Samuelsen, G. Shirane, and K. Hirakawa, Phys. Rev. **188**, 919 (1969).
[34] J. C. T. Lee, S. Yuan, S. Lal, Y. I. Joe, Y. Gan, S. Smadici, K. Finkelstein, Y. Feng, A. Rusydi, P. M. Goldbart, S. L. Cooper, and P. Abbamonte, Nature Phys. **8**, 63 (2012).